ACI STRUCTURAL JOURNAL TECHNICAL PAPER

Title No. 118-S133

Diagonally Reinforced Concrete Coupling Beams: Effects of Axial Restraint

by Ashwin Poudel, Shahedreen Ameen, Rémy D. Lequesne, and Andrés Lepage

Two pairs of nominally identical large-scale coupling beam specimens were tested under reversed cyclic displacements. Within each pair, one specimen was free to elongate and the other had resistance to elongation during testing. The specimens had clear span-to-overall-depth ratios of 1.9, a nominal concrete compressive strength of 6000 psi (42 MPa), Grade 60 or 120 (420 or 830) diagonal bars, and nominal shear stresses near the ACI Building Code (ACI 318) limit of $10\sqrt{f_c'}$ psi ($0.83\sqrt{f_c'}$ MPa). Passive axial restraint resulted in beam axial forces and was correlated with higher coupling beam strength, lower chord rotation capacity, earlier diagonal bar buckling, and greater damage. The importance of these effects increased with the magnitude of the induced axial force. The ACI equation for coupling beam nominal strength (based on the area, yield stress, and inclination of diagonal bars) underestimated beam strength by up to 80%, whereas estimates based on flexural strength were substantially more accurate and allowed consideration of axial force effects.

Keywords: axial force; axial restraint; chord rotation capacity; coupling beam strength; damage progression; high-strength reinforcement; reversed cyclic displacements.

INTRODUCTION

Reinforced concrete coupled structural walls are common components of lateral force-resisting systems. Deep and short coupling beams, which link adjacent structural walls, are often reinforced with diagonally oriented bars confined with closely spaced transverse reinforcement. Beams thus reinforced exhibit satisfactory strength, stiffness, and deformation capacity.[1,2] Several alternatives to diagonally reinforced beams have been investigated with the aim of reducing reinforcement congestion and easing construction, including different reinforcement arrangements,[3-10] fiber reinforcement,[11,12] high-strength reinforcement,[13-15] and use of steel sections.[16,17] However, diagonal reinforcement remains prevalent in practice.

In most of these prior experimental studies, the coupling beam specimens were free to elongate as inelastic bar strains and concrete damage accumulated. In others, the coupling beam was axially restrained, resulting in beam axial forces. The authors are not aware of tests of nominally identical coupling beams with and without axial restraint that can be used to quantify the importance of this variable.

In practice, structural walls and floor diaphragms passively resist coupling beam elongation, although the stiffness of this restraint and the magnitude of the resulting axial forces are unknown. Analytical studies[18-20] have indicated that the axial restraint present in buildings is likely sufficient to affect coupling beam strength and deformation capacity. Coupling beam overstrength resulting from axial restraint was also identified as a contributing cause of foundation damage observed in a coupled-wall structure following the 2010 and 2011 Canterbury earthquakes.[20]

The aim of this study was therefore to experimentally quantify the effects of passive axial restraint on coupling beam strength, deformation capacity, and extent of damage. This was done by comparing results from two pairs of specimens tested under reversed cyclic displacements. Within each pair of specimens, the only difference was the axial restraint provided during testing: one specimen was free to elongate, and the other was restrained axially. The unrestrained specimens were part of a study investigating the use of high-strength steel reinforcement in coupling beams.[13,14]

There are related questions that were outside the scope of this study. For instance, there is a need to quantify, in realistic structures, the stiffness of the resistance provided by walls and floor diaphragms to coupling beam axial elongation and to develop a means of estimating the resulting coupling beam axial forces. This study also does not address axial forces in coupling beams located near the base of a structure induced by the transfer of wall shear between piers,[21] which is independent of the axial restraint stiffness.

RESEARCH SIGNIFICANCE

Guidance for analysis and design of coupling beams do not consider axial restraint. However, field observations and analytical studies[18-20] have indicated that axial restraint may have important effects on coupling beam strength and deformation capacity. This study is needed because: 1) the authors are not aware of tests of nominally identical coupling beams with and without axial restraint that can be used to quantify the importance of passive axial restraint; and 2) there is no consensus among researchers and code writers on whether axial restraint should be provided in tests of coupling beams to characterize and quantify their seismic performance.

EXPERIMENTAL PROGRAM

Specimens

Two pairs of nominally identical large-scale coupling beam specimens were tested under reversed cyclic displacements. Each specimen consisted of a coupling beam (rotated 90 degrees from horizontal) framing into top and bottom blocks. The coupling beams had a clear span length of 34 in.

ACI Structural Journal, V. 118, No. 6, November 2021.
MS No. S-2020-513.R1, doi: 10.14359/51732991, received April 12, 2021, and reviewed under Institute publication policies.

Table 1—Summary of coupling beam specimens

ID	Diagonal bar f_y, ksi (MPa)	Design shear stress* $\sqrt{f'_c}$, psi (MPa)	Diagonal bars†	Longitudinal bars Grade 60 (420)
CB1	60 (420)	9.6 (0.80)	12 No. 7 (22)	8 No. 3 (10) Cutoff‡
CB1A	60 (420)	9.6 (0.80)	12 No. 7 (22)	8 No. 3 (10) Cutoff‡
CB2D	120 (830)	9.4 (0.78)	8 No. 6 (19)	8 No. 3 (10) Developed§
CB2AD	120 (830)	9.4 (0.78)	8 No. 6 (19)	8 No. 3 (10) Developed§

*Based on ACI 318-14,[22] Eq. (18.10.7.4), using f_y and f'_c = 6000 psi (41 MPa) and α = 18 degrees.

†Includes all bars from two groups of diagonals.

‡Cutoff 2 in. (50 mm) from beam-wall interface, consistent with ACI 318-14[22] Commentary R18.10.7.

§Developed into top and bottom blocks following Eq. (25.4.2.3a) in ACI 318-14[22] and bar stress of 1.25f_y.

(860 mm), overall depth of 18 in. (460 mm), and width of 10 in. (250 mm), resulting in a clear span-to-overall-depth ratio (ℓ_n/h) of 1.9. Details of the specimens are listed in Table 1 and shown in Fig. 1 and 2. The pair of specimens CB1 and CB1A were nominally equivalent, as were the other pair CB2D and CB2AD, with one difference: CB1A and CB2AD were restrained against axial elongation during testing, whereas CB1 and CB2D were free to elongate. The "A" in the specimen names denotes axial restraint, and the "D" denotes that the secondary longitudinal reinforcement was developed into the end blocks. Comparisons are made throughout this article within the nominally equivalent pairs of specimens to identify the effects of axial restraint.

The specimens were designed to resist a nominal shear stress of approximately $10\sqrt{f'_c}$ psi ($0.83\sqrt{f'_c}$ MPa), calculated assuming the diagonal reinforcement resists all imposed shear force. The diagonal reinforcement consisted of Grade 60 (420) bars in CB1 and CB1A and Grade 120

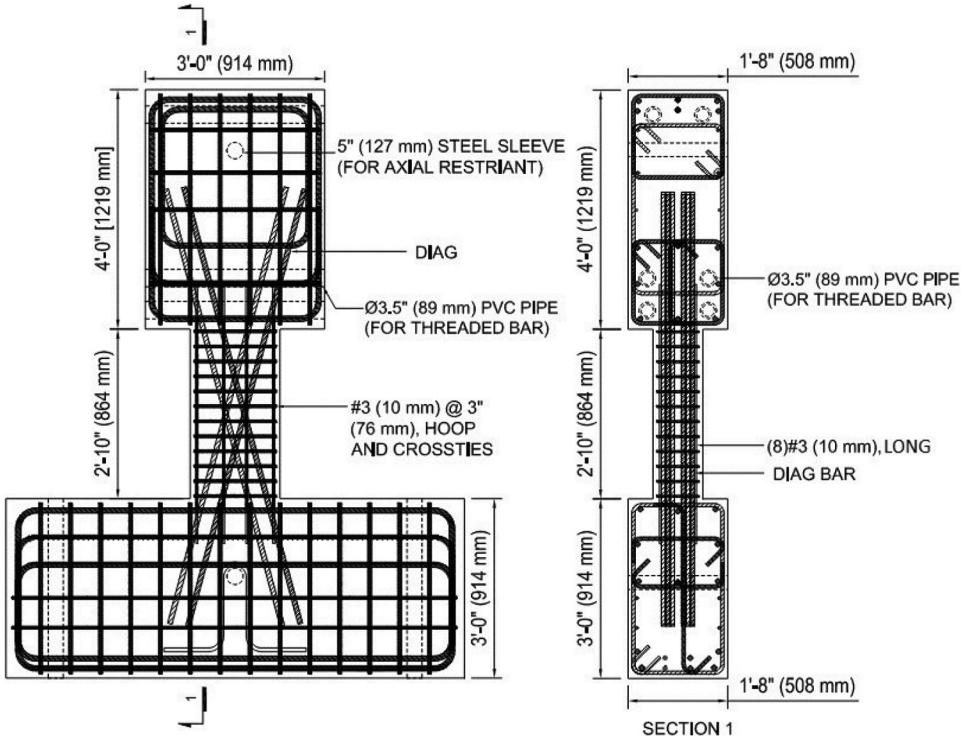

Fig. 1—Specimen details.

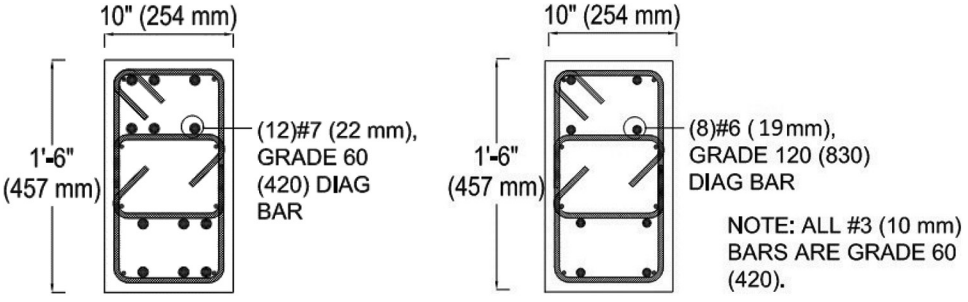

(a) CB1 and CB1A (b) CB2 and CB2AD

Fig. 2—Coupling beam cross sections near wall intersection.

(830) bars in CB2D and CB2AD. Secondary longitudinal reinforcement in all specimens consisted of eight No. 3 (10) Grade 60 (420 bars). Transverse reinforcement was nominally identical in all specimens, with No. 3 (10) Grade 60 (420) hoops and crossties spaced at 3 in. (75 mm) on center (Fig. 2), which was 3.4 and 4 times the diameter of the Grade 60 and 120 (420 and 830) diagonal bars, respectively. The transverse reinforcement area was within 5% of the values required in ACI 318-14,[22] Section 18.10.7.4d. The eight No. 3 (10) longitudinal bars in CB1 and CB1A were terminated 2 in. (50 mm) into the end blocks. In CB2D and CB2AD, the eight No. 3 (10) longitudinal bars were extended into the end blocks by a length sufficient to develop a bar stress of $1.25f_y$. Effects on behavior of these differences in detailing and diagonal bar grade are examined elsewhere.[13] This paper is focused on differences in behavior within the pairs of nominally equivalent specimens correlated with axial restraint. The end blocks were designed to simulate wall boundary elements and were reinforced with a dense cage of Grade 60 (420 MPa) steel.

Table 2—Measured material properties, beam strength, and chord rotation capacity

ID	Test day f_{cm}*, ksi (MPa)	Diagonal bar f_{ym}†, ksi (MPa)	ε_{su}‡, %	V^+_{max}§, kip (kN)	V^-_{max}‖, kip (kN)	v_{max}#, psi (MPa)	θ_{cap}**, %
CB1	6.0 (41)	63 (434)	12.8	182 (810)	184 (818)	13.2 (1.10)	7.1
CB1A	6.4 (44)	63 (434)	12.8	240 (1068)	244 (1085)	16.9 (1.41)	6.2
CB2D	6.3 (43)	128 (883)	5.3	204 (907)	194 (863)	14.3 (1.19)	5.3
CB2AD	5.6 (39)	128 (883)	5.3	228 (1014)	234 (1041)	17.4 (1.44)	5.3

*Mean result from three 4 x 8 in. (100 x 200 mm) concrete cylinders tested following ASTM C39.[23]

†For diagonal bars tested per ASTM A370,[24] based on 0.2%-offset method. No. 3 (10) longitudinal and transverse bars had f_{ym} = 69 and 68 ksi (476 and 469 MPa), respectively.

‡Reinforcement uniform elongation (strain at peak stress) as defined in ASTM E8.[25]

§Maximum measured shear force in positive loading direction.

‖Maximum measured shear force in negative loading direction.

#Normalized shear stress calculated using maximum of V^+_{max} and V^-_{max} divided by $(b_w h\sqrt{f_{cm}})$.

**Mean of maximum chord rotations attained in each loading direction while maintaining a shear force not less than 80% of V^+_{max} or V^-_{max}.

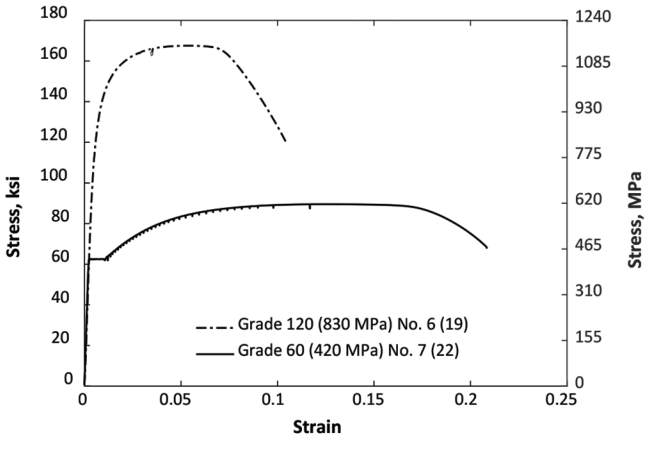

Fig. 3—Measured stress-versus-strain for diagonal reinforcing bars.

Materials

Measured material properties for both concrete and reinforcement are presented in Table 2. The specimens had ready mixed concrete from a local supplier with a target compressive strength of 6000 psi (41 MPa) and a maximum aggregate size of 0.5 in. (13 mm). Mixture proportions are reported elsewhere.[26,27]

Mill certifications for the Grade 60 (420) and Grade 120 (830) reinforcing bars showed compliance with ASTM A706[26] and ASTM A1035,[27] respectively. The mechanical properties of the steel were obtained from tensile tests in accordance with ASTM A370[28] and ASTM E8.[29] Figure 3 shows bar stress versus strain for samples of the diagonal reinforcing bars.

Test setup

Figure 4 shows the test setup. The bottom blocks of the specimens were bolted to the laboratory strong floor with two 2.5 in. (64 mm) diameter high-strength threaded rods. Two horizontal hydraulic actuators were used to load the specimens. The actuators each have a stroke length of 40 in. (1000 mm) and a force capacity of 220 kip (980 kN). The actuators were connected to the strong wall and specimen with a series of steel fixtures. Additional steel fixtures were used to brace the loading system out-of-plane.

In CB1A and CB2AD, 3 in. (76 mm) diameter high-strength threaded rods were placed parallel to the coupling beam centerline along both the front and the back faces of the specimens to connect the top and bottom blocks and restrain beam elongation during testing (Fig. 4). These 3 in. (76 mm) diameter rods were connected to 5 in. (12 mm) diameter Grade 50 (340 MPa) solid steel rods that passed through the top and bottom blocks. The 5 in. (127 mm) diameter rods passed through steel pipes embedded in the top and bottom blocks (shown with dashed circles in Fig. 1). The steel pipes had outer diameters of 6.63 in. (168 mm) and inner diameters of 6.07 in. (154 mm). During assembly, the 5 in. (127 mm) diameter rods were greased to facilitate free rotation during testing with respect to both the steel pipe and the fixtures at the ends of the 3 in. (76 mm) diameter threaded rods. Before testing, nuts on the 3 in. (76 mm) diameter rods

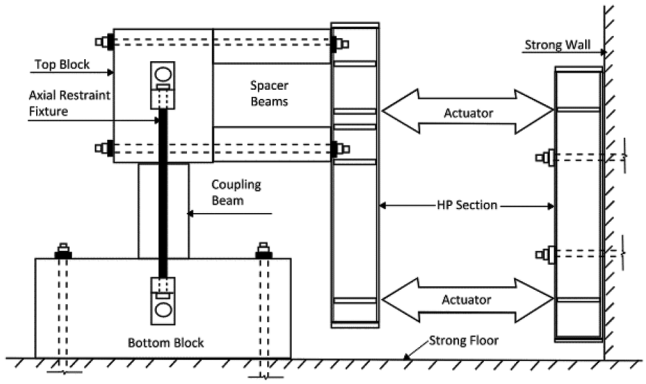

Fig. 4—Test setup.

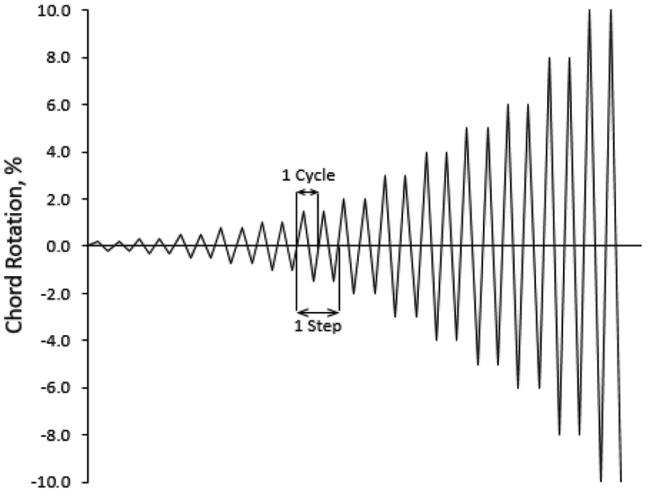

Fig. 5—Loading protocol.

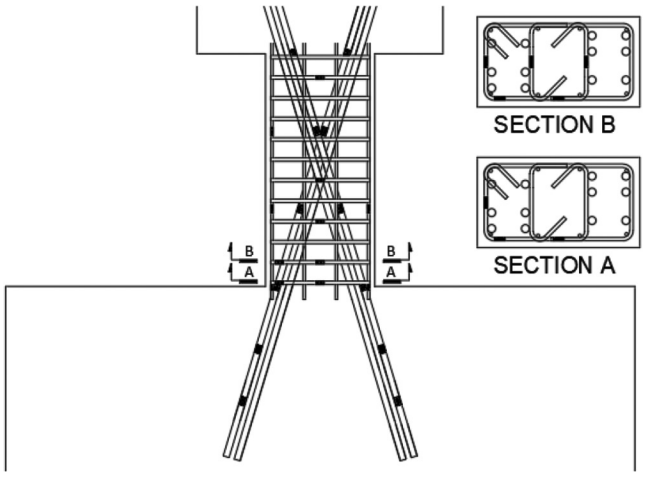

Fig. 6—Strain gauge layout.

were lightly tightened until the 5 in. (127 mm) diameter rods were in contact with the inner walls of the steel pipes in both the top and bottom blocks but without imposing axial force on the coupling beam.

Loading protocol

Specimens were subjected to a series of reversed cyclic displacements following the protocol shown in Fig. 5. Force-based control was used up to 0.9 times the force associated with anticipated bar yielding and displacement-based control was used thereafter. The ratio between forces or displacements applied by the two actuators was selected such that a zero-moment inflection point occurred near beam midspan, resulting in double-curvature bending throughout the tests.

Instrumentation

Diagonal, transverse, and longitudinal reinforcing bars were instrumented with 28 electrical resistance strain gauges placed at the locations shown in Fig. 6. Six strain gauges were attached to two diagonal bars each, 11 strain gauges were attached to hoops and ties, and five strain gauges were attached to No. 3 (10) longitudinal bars. Four strain gauges were attached to each 3 in. (76 mm) diameter threaded rod to record axial strain so the corresponding axial force induced

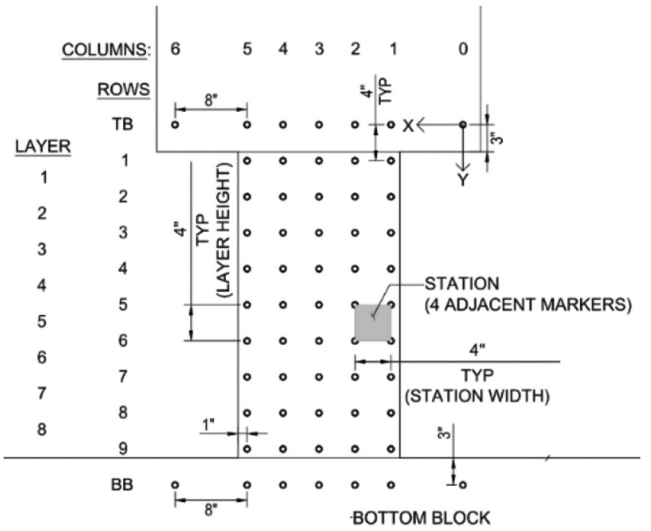

Fig. 7—Locations of optical markers.

in the specimen could be calculated. These strain gauges were aligned with the longitudinal axis of the threaded rods and spaced evenly along their length. All strain gauges were rated for 15% strain.

Deformations and displacements were measured using an infrared-based noncontact measurement system that recorded the position of optical markers on the surface of the specimens (Fig. 7). The markers emit infrared light pulses that are detected by cameras, allowing their spatial coordinates to be triangulated and recorded at a selected frequency. The markers were attached to the concrete in a square grid over one face of the specimen and part of the top and bottom blocks.

EXPERIMENTAL RESULTS AND DISCUSSION

Overall specimen response

Plots of measured shear versus chord rotation are shown in Fig. 8. The shear force was measured using actuator load cells. Chord rotation was calculated using data from the infrared-based noncontact position measurement system as the relative horizontal displacement (x-axis component in Fig. 7) between the top and bottom blocks, adjusted for rotation of the top and bottom blocks (refer to References 23 and 24 for details). Table 2 lists the maximum shear force, V_{max}, in each loading direction and the average chord rotation capacity, θ_{cap}, for each specimen. The chord rotation capacity of a specimen was defined as the mean of the maximum chord rotations imposed in each loading direction before strength diminished to less than 80% of V_{max} in each loading direction.

The specimens exhibited maximum shear stresses between 13.2 and 17.4 $\sqrt{f_{cm}}$ psi (1.10 and 1.44 $\sqrt{f_{cm}}$ MPa). Within both specimen pairs, the axially restrained specimen exhibited the higher strength: in terms of force, CB1A was approximately 30% stronger than CB1, and CB2AD was approximately, 15% stronger than CB2D.

Chord rotation capacities, θ_{cap}, were 7.1% and 6.2% for CB1 and CB1A, respectively, and 5.3% for both CB2D and CB2AD. There was a reduction in θ_{cap} associated with axial restraint among the Grade 60 (420) specimens but not

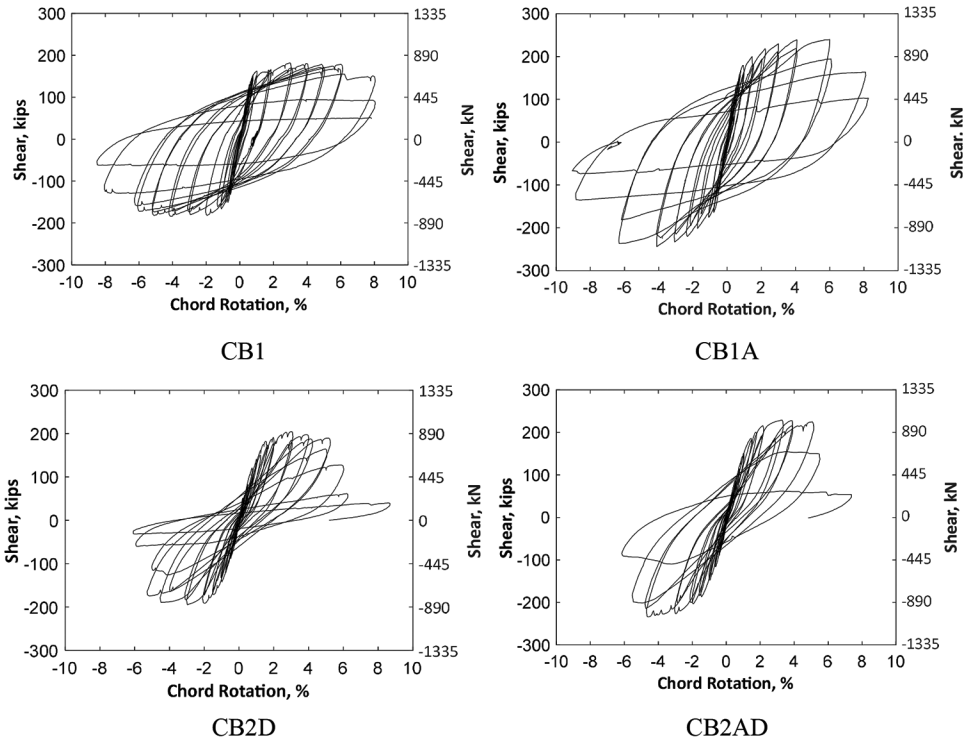

Fig. 8—Shear versus chord rotation.

among the Grade 120 (830) specimens. The effects of axial restraint on chord rotation capacity are discussed in more depth later. The effects of reinforcement grade and detailing on θ_{cap} are reported elsewhere.[13]

Progression of damage

In all four specimens, horizontal flexural cracks associated with double-curvature bending were observed on the 10 in. (250 mm) wide faces of the beams starting at chord rotation demands near 0.2%. These horizontal cracks continued onto the 18 in. (460 mm) wide face and became inclined as loading progressed. New cracks continued to develop and extend until chord rotation demands near 4%, after which existing cracks continued to widen, but new cracks were not observed.

Figure 9 shows the specimens after completion of the cycles to 4% chord rotation. There was cracking throughout the beam spans and concentrated damage near the beam ends—particularly in CB1 and CB1A, which had the secondary No. 3 (10) longitudinal bars cut off near the beam ends. Before the tests were terminated, the specimens all exhibited concrete spalling and diagonal bar buckling near the specimen corners, and CB1 and CB1A exhibited diagonal bar fracture at the beam ends. A comparison of Fig. 9(a) with 9(b) and also Fig. 9(c) with 9(d), shows that the axially restrained specimens exhibited more extensive spalling than the unrestrained specimens. This might be attributed to the compression forces induced by the axial restraint.

Table 3 identifies the target chord rotation cycles when bar buckling or bar fracture was first observed during the tests. As is frequently the case,[13,15,26] Table 3 shows that diagonal bar buckling preceded diagonal bar fracture. It also shows that diagonal bars fractured in both CB1 and CB1A, whereas

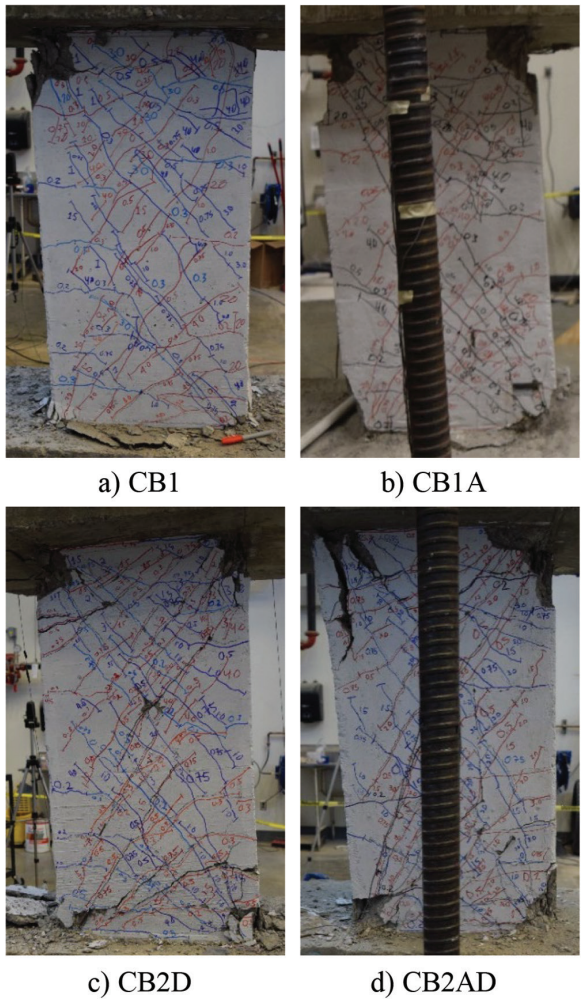

Fig. 9—Coupling beam condition after chord rotation cycles to 4%.

Table 3—Chord rotation cycles when bar buckling or bar fracture was first observed

ID	Bar type	Target chord rotation cycle													
		4%				5%				6%				8%	
		i+	i–	ii+	ii–	i+	i–	ii+	ii–	i+	i–	ii+	ii–	i+	i–
CB1	Diagonal	—	—	—	—	—	—	—	—	—	B	—	—	F	—
	Longitudinal	—	—	—	—	—	B	—	—	—	—	—	—	F	—
CB1A	Diagonal	—	—	—	B	—	—	—	—	—	—	—	—	F	—
	Longitudinal	—	—	—	B	—	—	—	—	—	—	—	—	F	—
CB2D	Diagonal	—	—	—	—	—	—	—	B	—	—	—	—	—	—
	Longitudinal	—	—	—	—	F	—	—	—	—	—	—	—	—	—
CB2AD	Diagonal	—	—	—	—	—	—	B	—	—	—	—	—	—	—
	Longitudinal	—	—	—	—	—	—	B	—	—	—	—	—	—	—

Note: i+ is first cycle in positive loading direction; i– is first cycle in negative loading direction; ii+ is second cycle in positive loading direction; ii– is second cycle in negative loading direction; B is buckling of reinforcement; F is fracture of reinforcement.

none of the diagonal bars in CB2D and CB2AD fractured. This is attributable to the longitudinal bar detailing: developing the longitudinal reinforcement beyond the beam-wall interface reduced beam-end rotation demands and therefore delayed or prevented diagonal bar fracture.

With respect to the effect of axial restraint, Table 3 shows that within each pair of nominally equivalent specimens, diagonal bar buckling occurred earlier in specimens with axial restraint. This difference was large for CB1 and CB1A (diagonal bar buckling was first observed in the first cycle to 6% chord rotation and the second cycle to 4% chord rotation in CB1 and CB1A, respectively). The difference was small for CB2D and CB2AD (diagonal bar buckling was first observed in the fourth and third half-cycles to 5% in CB2D and CB2AD, respectively).

The presence of axial restraint therefore correlated with earlier and more extensive concrete spalling and bar buckling. This difference was most dramatic between CB1 and CB1A and less so between CB2D and CB2AD.

Beam elongation and axial force

Figure 10 shows beam elongation versus chord rotation for each beam. In CB1 and CB2D, elongation was calculated as the relative vertical displacement (y-axis component in Fig. 7) between the middle markers on the top and bottom blocks (markers TB-3 and BB-3 in Fig. 7) divided by the nominal beam clear span. Because the axial restraint system obstructed the view of the two middle markers in tests of the axially restrained beams, elongation was calculated for CB1A and CB2AD using the average y-axis positions of markers adjacent to the middle marker on the top and bottom blocks.

Figure 10 shows that beam elongations tended to increase as chord rotation increased up to approximately 6% chord rotation for CB1 and CB1A and 5% chord rotation for CB2D and CB2AD, after which the beams tended to shorten. This shift to shortening coincided with extensive concrete spalling and bar buckling and occurred after the beams reached their strengths. CB1 had the highest elongation (2.5%), CB1A and CB2D both had maximum elongations of 1%, and CB2AD had the lowest peak elongation (0.6%). This ranking of beams was the same at chord rotations of 4%, with maximum elongations of 1.8%, 0.9%, 0.9%, and 0.5%. This indicates that: 1) specimens with Grade 60 (420) reinforcement and bars terminated near the beam ends (CB1 and CB1A) tended to have higher elongations than the specimens with Grade 120 (830) reinforcement and all longitudinal reinforcement developed at the beam ends (CB2D and CB2AD); and 2) the axial restraint present for these tests caused a reduction in elongation of approximately 50% within both pairs of nominally equivalent specimens.

Figure 11 shows beam axial force versus chord rotation for the axially restrained beams (CB1A and CB2AD). The axial force was based on data from strain gauges affixed to each of the 3 in. (76 mm) diameter threaded rods (axial restraint fixture in Fig. 4). The measured strains were converted to force using a modulus of 29,000 ksi (200 GPa) and the nominal rod area of 6.85 in.^{2} (4420 mm^2), assuming zero axial force at the start of the tests. Beam axial force was taken as the sum of forces in the two rods neglecting the effects of lateral displacements on the rod orientation (the length of the restraining rods was 2.5 times the coupling beam clear span). Forces in each of the rods were approximately equal during each test.

Axial forces were near zero for chord rotations up to approximately 1%. At chord rotations between 4 and 6%, axial forces reached approximately 220 and 110 kip (980 and 480 kN) in CB1A and CB2AD, corresponding to approximately $0.2A_g f_{cm}$ and $0.1A_g f_{cm}$, respectively. These axial forces are large enough to increase member strength and decrease deformation capacity, particularly in CB1A. Because axial forces were small for chord rotations up to approximately 1.5%, coupling beam initial stiffness was not affected by axial restraint.

Stiffness of axial restraint

Figure 12(a) shows axial force versus beam elongation from the test of CB1A. The figure shows that axial force tended to increase with elongation but that the relationship was not linear in these tests. Rather, axial force tended to remain small, less than approximately 20 kip (90 kN), for elongations up to approximately 0.1 in. (2.5 mm) and

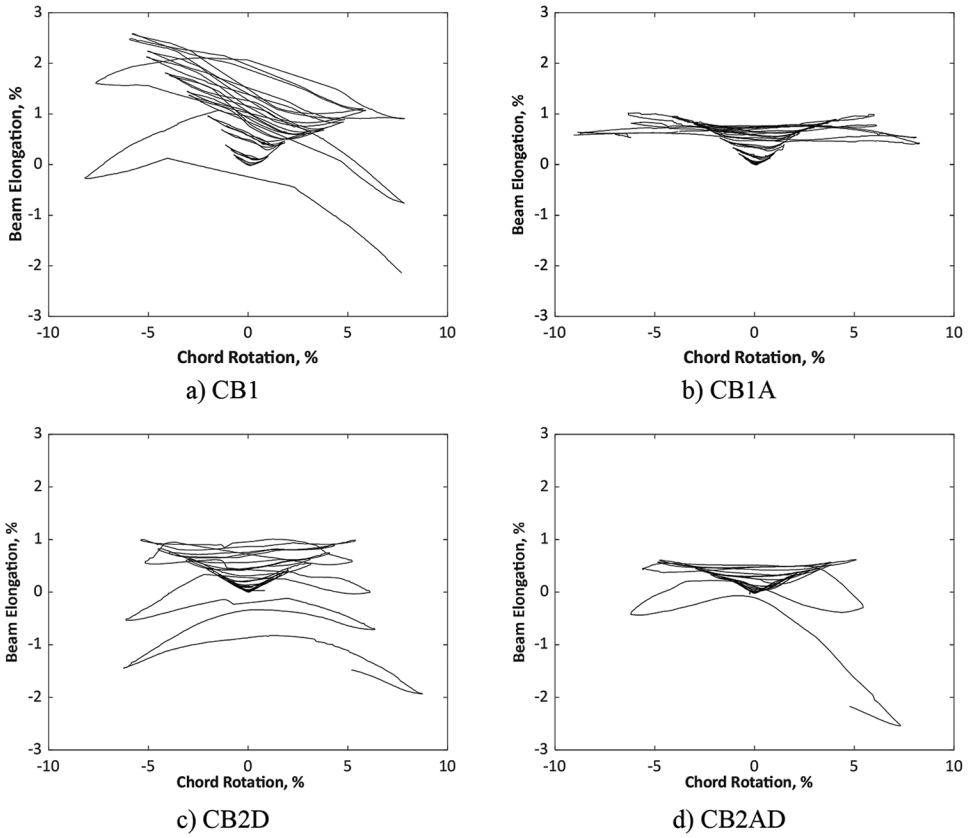

Fig. 10—Beam elongation versus chord rotation.

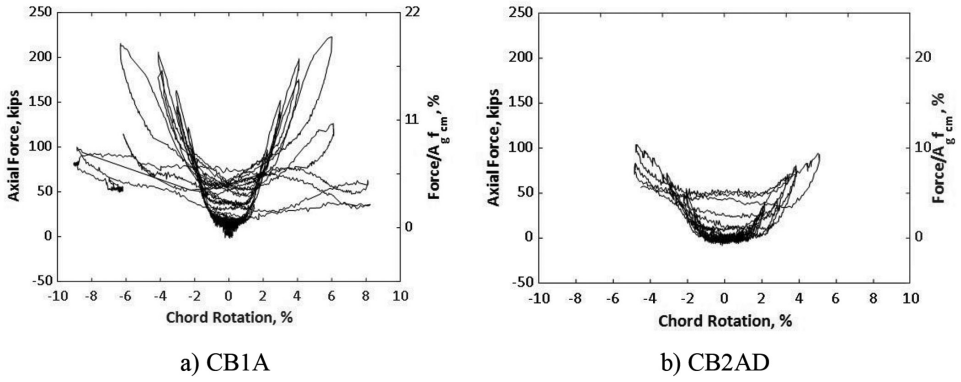

Fig. 11—Axial force versus chord rotation. (Note: 1 kip = 4.45 kN.)

increased thereafter. As chord rotations increased within each loading cycle, the slope of the axial force-elongation data approached 1000 kip/in. (175 kN/mm). The unloading slope tended to be higher than the reloading slope, resulting in a ratcheting effect that caused the elongation for a given axial force to increase with the amplitude and number of cycles.

One way to compare the stiffness of the axial restraint provided to the two restrained beams is with envelopes of the axial force-elongation data drawn to the peak of each cycle (Fig. 12(b)). The envelopes followed a similar path up to an elongation of approximately 0.2 in. (5 mm), where both beams experienced axial forces between 80 and 100 kip (360 and 440 kN). The beams, however, reached this level of axial force at different points in the test: near 2% and 5% chord rotation for CB1A and CB2AD, respectively. The average slope of the axial force versus elongation envelopes, for elongation between 0.1 and 0.2 in. (2.5 and 5 mm), was nearly the same for CB1A and CB2AD. This indicates that the axial restraint system was similarly stiff for both specimens but that some other factor led to a lower elongation in CB2AD. This interpretation is supported by a comparison of the elongations for the unrestrained beams (CB1 and CB2D) in Fig. 10(a) and (c), where CB1 elongated more than CB2D. It is not clear whether this is attributable to the difference in reinforcement ratio, diagonal bar grade, or longitudinal reinforcement detailing near the wall face.

Chord rotation capacity

As described previously, Table 2 shows that θ_{cap} was smaller for the axially restrained specimen in the CB1-CB1A pair but not in the CB2D-CB2AD pair. To examine whether this finding is sensitive to the definition of chord rotation capacity, two other definitions were considered. Table 4

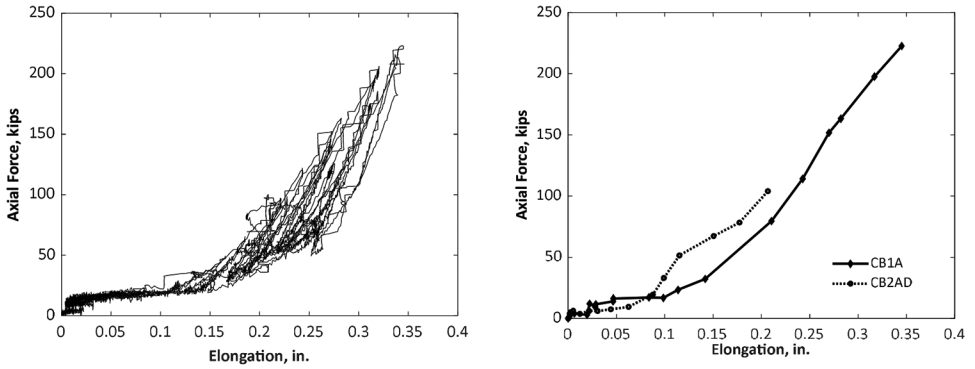

a) CB1A b) Envelopes

Fig. 12—Axial force versus beam elongation. (Note: 1 kip = 4.45 kN.)

Table 4—Chord rotation capacity based on three definitions

ID	θ_{cap}*, %	$\theta_{cap,I}$*, %	$\theta_{cap,\ II}$*, %	Mean, %
CB1	7.1	7.5	7.5	7.4
CB1A	6.2	7.3	6.7	6.7
CB2D	5.3	5.6	5.6	5.5
CB2AD	5.3	5.4	5.4	5.4

*Refer to the Notation section.

shows θ_{cap}, $\theta_{cap,I}$, and $\theta_{cap,II}$ for each specimen, where all three refer to the highest chord rotation attained before strength decreased to less than $0.8V_{max}$ but differ on which shear versus chord rotation relationship is used to determine the chord rotation associated with $0.8V_{max}$. Refer to the Notation section for detailed definitions. The values shown in Table 4 are the mean of values obtained in the positive and negative loading directions for all three definitions of chord rotation capacity.

Table 4 shows that although the three chord rotation capacity definitions produced somewhat different values—especially for CB1A—the ranking of beams persisted. The mean chord rotation capacity shown in the last column of Table 4 indicates that axial restraint resulted in reduced chord rotation capacities; 0.7 and 0.1 percentage point decreases for the CB1-CB1A pair and CB2D-CB2AD pair, respectively. These reductions represent 9% and 2% of the chord rotation capacities for the beams without axial restraint.

These results indicate that axial restraint can produce reductions in deformation capacity but that the importance of the reduction depends on the axial force induced in the beam, as expected. The 9% and 2% reductions in chord rotation capacity occurred in beams with maximum axial forces of approximately $0.2A_g f_{cm}$ and $0.1A_g f_{cm}$, respectively.

Beam strength

As described previously, both axially restrained beams were stronger than their respective axially unrestrained control beams: CB1A was 30% stronger than CB1, and CB2AD was 15% stronger than CB2D. It is not surprising that the beam with the larger axial force (CB1A) had the larger increase in strength, because both axially restrained beams underwent axial forces that were less than the axial force associated with balanced strain conditions.

Table 5—Measured beam strengths and measured-to-calculated strength ratios

		Measured-to-calculated strength ratios				
		Method 1*		Method 2†		
ID	V_{max}, kip (kN)	(a)	(b)	(a)	(b)	Method 3‡
CB1	184 (818)	1.38	1.31	1.11	1.07	0.89
CB1A	244 (1085)	1.83	1.74	1.47	1.42	1.19
		—	—	1.12§	1.07§	0.99§
CB2D	204 (907)	1.56	1.47	1.18‖	1.12‖	1.02‖
CB2AD	234 (1041)	1.79	1.68	1.36‖	1.28‖	1.17‖
		—	—	1.25‖,#	1.25‖,#	1.23‖,#

*Calculated nominal shear strength based on ACI 318-14,[22] Eq. (18.10.7.4) (Eq. (1)) using α = 18 degrees and (a) f_y; and (b) f_{ym}.

†Shear force corresponding to M_n calculated using: (a) f_y and f_c'; and (b) f_{ym} and f_{cm}.

‡Shear force corresponding to M_{pr} calculated using tensile reinforcement stress of $1.25f_y$ and f_{cm}.

§Includes axial force of 200 kip (890 kN).

‖Includes contribution of eight No. 3 (10) Grade 60 (420) longitudinal bars developed into end blocks.

#Includes axial force of 100 kip (440 kN).

Table 5 shows the measured strength of each beam and the ratio of measured-to-calculated strength based on three calculation methods. Method 1 is the nominal shear strength determined in accordance with ACI 318-14,[22] Eq. (18.10.7.4), shown later as Eq. (1); Method 2 is the shear force corresponding to development of the nominal flexural strength, M_n, at both ends of the beam; and Method 3 is the shear force corresponding to development of the probable flexural strength, M_{pr}, at both ends of the beam (calculated based on f_{cm} for concrete and $1.25f_y$ for tensile reinforcement). To calculate the flexural strength (Methods 2 and 3), a concrete stress block of 0.85 times the concrete compressive strength was assumed, and the contribution of the reinforcement accounted for the inclination of diagonal bars. In CB1 and CB1A, the contribution of the non-diagonal longitudinal bars was neglected because the bars were terminated near the beam-wall interface. For Methods 1 and 2, separate measured-to-calculated strength ratios are provided for either specified or measured material properties (f_y and f_c' or f_{ym} and f_{cm}).

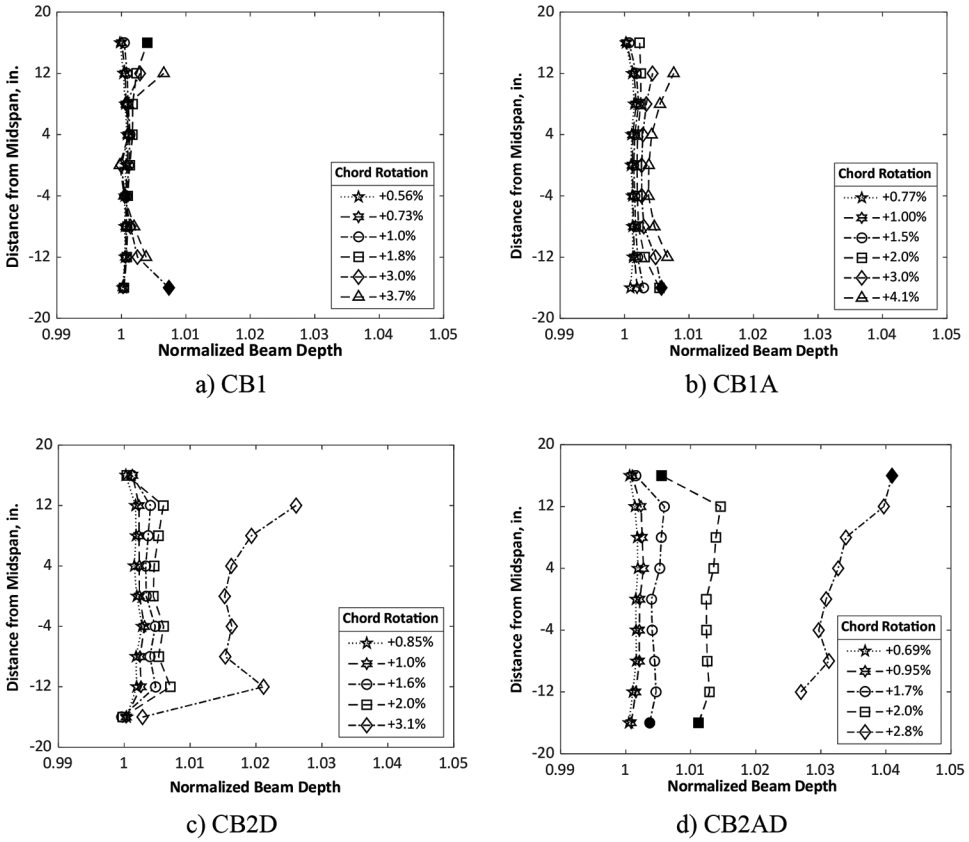

Fig. 13—Beam expansion for selected chord rotations. (Note: 1 kip = 4.45 kN.)

$$V_n = 2A_{vd} f_y \sin\alpha \quad (1)$$

The measured-to-calculated strength ratios in Table 5 show that the measured strength was greater than the nominal strength (Method 1a) by approximately 40% and 80% for CB1 and CB1A, respectively. The ACI Building Code[22] design equation (Eq. (1)) therefore considerably underestimates the strength of conventional diagonally reinforced coupling beams, particularly if axial restraint is present. The measured-to-calculated strength ratio was larger for CB2D, which had Grade 120 (830) diagonal bars. The accuracy of Method 1b, based on measured reinforcement yield stress, was only marginally better, indicating that material overstrength does not account for most of the observed overstrength. Method 2 provided improved estimates of strength using either specified or measured material properties, consistent with prior findings.[15,30] Based on Method 2b and considering axial forces, the measured strength was greater than the calculated strength by approximately 10% for CB1 and CB1A, and 20% for CB2D and CB2AD. Method 3 provided the most accurate estimate of beam strength, although it overpredicted the strength of CB1 by approximately 10%. Axial forces close to the maximum measured during testing were used because they occurred near the maximum applied shear.

Table 5 shows that for either Method 2 or 3 the calculated strengths for axially restrained specimens are generally more accurate when the maximum axial forces measured during testing are considered.

Normalized beam depth

Data from markers glued to the surface of the concrete (Fig. 7) were used to calculate changes in normalized beam depth along the beam span. Figure 13 shows normalized beam depths for loading to positive chord rotations (similar results were obtained for loading to negative chord rotations). Normalized beam depth, a proxy for expansion of the beam core and damage, was calculated as the change in relative distance between the two outermost markers in each row (Fig. 7), divided by the initial distance between the markers. It was calculated at the peak chord rotation in the second cycle to each target chord rotation (Fig. 5). Typically, the outermost markers were those located in Columns 1 and 5 (Fig. 7), but in the case of a marker malfunction, adjacent markers from other columns were used. Open symbols in Fig. 13 represent marker data based on Columns 1 and 5, whereas solid symbols represent data based on adjacent columns.

Changes in the depth of CB1, a specimen with secondary (nondiagonal) longitudinal reinforcement terminated near the beam-block interfaces, were small (≤0.25% and ≤0.3% up to chord rotations of approximately 3 and 4% in the five rows nearest midspan). CB1A, the nominally equivalent specimen with axial restraint, exhibited larger changes in beam depth than CB1 (≤0.6% and ≤0.8% up to chord rotations of approximately 3 and 4%).

For CB2D, a specimen with developed secondary (nondiagonal) longitudinal reinforcement, changes in beam depth were generally larger than in CB1 and CB1A, indicating that damage was more extensive as a result of deformations

moving away from the beam ends and into the span. Changes in the depth of CB2D reached 2.8% for chord rotations of approximately 3%. The axially restrained specimen, CB2AD, showed larger changes in beam depth than all other beams, with values predominantly between 3 and 4% for chord rotations of approximately 3%.

The changes in beam depth, an indirect measure of core expansion and beam damage, support the observation that axially restrained beams exhibited greater damage than axially unrestrained beams at similar chord rotation demands. The greater core expansion combined with the observation that diagonal reinforcement buckled earlier in axially restrained beams may explain why chord rotation capacities tended to be lower in axially restrained beams.

SUMMARY AND CONCLUSIONS

The effects of passive axial restraint on coupling beam behavior were examined on the basis of tests of two pairs of nominally equivalent specimens. The specimens had a clear span-to-overall depth ratio of 1.9, a nominal concrete compressive strength of 6000 psi (42 MPa), Grade 60 or 120 (420 or 830) diagonal bars, and nominal shear stresses near the ACI Building Code limit of $10\sqrt{f_c'}$, psi ($0.83\sqrt{f_c'}$ MPa). Within each pair, one specimen was free to elongate during testing, whereas the other was restrained axially. Results support the following conclusions:

1. Axial restraint was correlated with higher coupling beam strength, lower chord rotation capacity, earlier diagonal bar buckling, and greater damage at chord rotations of 3 and 4%.

2. The importance of the effects of axial restraint on strength, chord rotation capacity, and damage was correlated with the magnitude of the induced axial force. The beam (CB1A) with a maximum axial force near $0.2A_gf_{cm}$ had 30% more strength, 9% less chord rotation capacity, and diagonal bar buckling occurring three loading cycles earlier than in the unrestrained specimen. The beam (CB2AD) with a maximum axial force near $0.1A_gf_{cm}$ had 15% more strength, a negligible (2%) difference in chord rotation capacity, and diagonal bar buckling occurring one-half cycle earlier than in the unrestrained specimen.

3. Coupling beam reinforcement ratio, detailing, and grade appear to affect the tendency of a coupling beam to elongate and therefore the magnitude of the axial force induced by restraint. Both restrained beams were designed for similar strengths and were tested with the same restraint system, but the beam (CB1A) with Grade 60 (420) diagonal bars and nondiagonal reinforcement terminated near the beam-wall interfaces had axial forces that were twice as large as the beam (CB2AD) with Grade 120 (830) diagonal bars and developed nondiagonal reinforcement.

4. Measured beam strengths exceeded their nominal strengths based on Eq. (1) by approximately 40 to 60% in the unrestrained specimens and 80% in the axially restrained specimens. Beam strength was more accurately estimated using either nominal or probable flexural strengths calculated at the beam ends and accounting for induced axial forces. Measured-to-calculated strength ratios were between 1.0 and 1.3 based on nominal flexural strengths (calculated using f_{cm}, f_{ym}, and measured axial forces) and between approximately 0.9 and 1.2 based on probable flexural strengths (calculated using f_{cm}, $1.25f_y$, and measured axial forces).

5. Effects of passive axial restraint on coupling beam stiffness appear negligible. In both axially restrained specimens, axial forces were less than approximately $0.05A_gf_{cm}$ (up to chord rotations of 1.5%), which is too small to affect beam stiffness. Axial forces also varied considerably within loading cycles and reached maximum values only near the peak chord rotations.

FUTURE WORK

Further investigation is recommended to address several important questions that were outside the scope of this study. These include the following: 1) assessing whether the stiffness of the axial restraint provided in these tests is representative of the restraint from adjoining structural walls and floor diaphragms present in buildings; 2) investigating the role of coupling beam aspect ratio and reinforcement ratio, detailing, and grade in the development of axial forces in axially restrained coupling beams; and 3) quantifying the effects on coupling beam behavior of axial forces caused by the shifting of shear forces between coupled walls near the base of structures.

AUTHOR BIOS

ACI member **Ashwin Poudel** *is a Project Consultant at Simpson Gumpertz & Heger Inc., New York, NY. He received his BS in civil engineering from Tribhuvan University, Kathmandu, Nepal, in 2014 and his MS from the University of Kansas, Lawrence, KS, in 2018.*

Shahedreen Ameen *is a Project Consultant at Simpson Gumpertz & Heger Inc., New York. She received her BS from Bangladesh University of Engineering and Technology, Dhaka, Bangladesh, in 2007 and her PhD from the University of Kansas in 2019.*

ACI member **Rémy D. Lequesne** *is an Associate Professor at the University of Kansas. He is Chair of Joint ACI-ASCE Committee 408, Bond and Development of Steel Reinforcement, and a member of Joint ACI-ASCE Committee 352, Joints and Connections in Monolithic Concrete Structures, and ACI Subcommittee 318-J, Joints and Connections (Structural Concrete Building Code).*

Andrés Lepage, *FACI, is a Professor at the University of Kansas. He is a member of ACI Committees 318, Structural Concrete Building Code; 335, Composite and Hybrid Structures; 374, Performance-Based Seismic Design of Concrete Buildings; and 375, Performance-Based Design of Concrete Buildings for Wind Loads.*

ACKNOWLEDGMENTS

Primary financial support was provided by the Department of Civil, Environmental & Architectural Engineering and the School of Engineering at the University of Kansas. Partial support was provided by MMFX Technologies Corporation and Commercial Metals Company.

NOTATION

A_g	=	beam gross cross-sectional area, in.^{2} (mm^2)
A_{vd}	=	total area of reinforcement in each group of diagonal bars in a diagonally reinforced coupling beam, in.^{2} (mm^2)
b_w	=	beam width, in. (mm)
f_c'	=	specified concrete compressive strength, psi (MPa)
f_{cm}	=	measured concrete compressive strength, psi (MPa)
f_y	=	specified reinforcement yield stress, ksi (MPa)
f_{ym}	=	measured reinforcement yield stress, ksi (MPa)
h	=	overall beam depth, in. (mm)
ℓ_n	=	beam clear span measured face-to-face of supports, in. (mm)
M_n	=	nominal moment strength, in.·kip (kN·m)
M_{pr}	=	probable moment strength, in.·kip (kN·m)
V_{max}	=	larger of V^+_{max} and V^-_{max}, kip (kN)

V^+_{max} = largest magnitude shear force in positive loading direction, kip (kN)

V^-_{max} = largest magnitude shear force in negative loading direction, kip (kN)

v_{max} = normalized shear stress calculated as $V_{max}/(b_w h\sqrt{f_{cm}})$, psi (MPa)

α = angle between diagonal bars and beam longitudinal axis

ε_{su} = reinforcement uniform elongation (strain at peak stress) measured in accordance with ASTM E8[29]

θ_{cap} = mean of maximum chord rotations attained in each loading direction while maintaining a shear force of not less than 80% of V^+_{max} or V^-_{max}. Not based on derived envelope

$\theta_{cap,I}$ = mean of chord rotations (in each loading direction) obtained from shear-chord rotation envelope intersecting 80% of maximum applied shear (V^+_{max} and V^-_{max}). Envelope was defined using first cycle of each loading step

$\theta_{cap,II}$ = mean of chord rotations (in each loading direction) obtained from shear-chord rotation envelope intersecting 80% of maximum applied shear (V^+_{max} and V^-_{max}). Envelope was defined using maximum chord rotation of each loading step (which includes two cycles)

REFERENCES

1. Paulay, T., and Binney, J. R., "Diagonally Reinforced Coupling Beams of Shear Walls," *Shear in Reinforced Concrete—Volume 1 and 2*, SP-42, American Concrete Institute, Farmington Hills, MI, Jan. 1974, pp. 579-598.

2. Naish, D.; Fry, A.; Klemencic, R.; and Wallace, J., "Reinforced Concrete Coupling Beams—Part I: Testing," *ACI Structural Journal*, V. 110, No. 6, Nov.-Dec. 2013, pp. 1057-1066.

3. Shiu, K. N.; Barney, G. B.; Fiorato, A. E.; and Corley, W. G., "Reversing Load Tests of Reinforced Concrete Coupling Beams," *Proceedings*, Central American Conference on Earthquake Engineering, San Salvador, El Salvador, 1978, pp. 239-249.

4. Tegos, I. A., and Penelis, G. G., "Seismic Resistance of Short Columns and Coupling Beams Reinforced with Inclined Bars," *ACI Structural Journal*, V. 85, No. 1, Jan.-Feb. 1988, pp. 82-88.

5. Tassios, T. P.; Moretti, M.; and Bezas, A., "On the Behavior and Ductility of Reinforced Concrete Coupling Beams of Shear Walls," *ACI Structural Journal*, V. 93, No. 6, Nov.-Dec. 1996, pp. 711-720.

6. Galano, L., and Vignoli, A., "Seismic Behavior of Short Coupling Beams with Different Reinforcement Layouts," *ACI Structural Journal*, V. 97, No. 6, Nov.-Dec. 2000, pp. 876-885.

7. Lim, E.; Hwang, S.-J.; Wang, T.-W.; and Chang, Y.-H., "An Investigation on the Seismic Behavior of Deep Reinforced Concrete Coupling Beams," *ACI Structural Journal*, V. 113, No. 2, Mar.-Apr. 2016, pp. 217-226. doi: 10.14359/51687939

8. Choi, Y.; Hajyalikhani, P.; and Chao, S.-H., "Seismic Performance of Innovative Reinforced Concrete Coupling Beam—Double-Beam Coupling Beam," *ACI Structural Journal*, V. 115, No. 1, Jan. 2018, pp. 113-125. doi: 10.14359/51700951

9. Cheng, M.-Y.; Gitomarsono, J.; and Zeng, H.-Y., "Cyclic Test of Diagonally Reinforced Concrete Coupling Beam with Different Shear Demand," *ACI Structural Journal*, V. 116, No. 6, Nov. 2019, pp. 241-250. doi: 10.14359/51718010

10. Weber-Kamin, A.; Ameen, S.; Lequesne, R. D.; and Lepage, A., "Database of Diagonally-Reinforced Concrete Coupling Beams (PRJ-3053)," DesignSafe-CI, 2021. doi: 10.17603/ds2-46wc-n185

11. Lequesne, R. D.; Parra-Montesinos, G. J.; and Wight, J. K., "Seismic Behavior and Detailing of High-Performance Fiber-Reinforced Concrete Coupling Beams and Coupled Wall Systems," *Journal of Structural Engineering*, ASCE, V. 139, No. 8, 2013, pp. 1362-1370. doi: 10.1061/(ASCE)ST.1943-541X.0000687

12. Parra-Montesinos, G. J.; Wight, J. K.; and Setkit, M., "Earthquake-Resistant Coupling Beams without Diagonal Reinforcement," *Concrete International*, V. 32, No. 12, Dec. 2010, pp. 36-40.

13. Ameen, S.; Lequesne, R. D.; and Lepage, A., "Diagonally Reinforced Concrete Coupling Beams with Grade 120 (830) High-Strength Steel Bars," *ACI Structural Journal*, V. 117, No. 6, Nov. 2020, pp. 199-210. doi: 10.14359/51728067

14. Ameen, S.; Lequesne, R. D.; and Lepage, A., "Diagonally-Reinforced Concrete Coupling Beams with High-Strength Steel Bars (PRJ-3077)," DesignSafe-CI, 2021. doi: 10.17603/ds2-dv8n-yx58

15. Weber-Kamin, A. S.; Lequesne, R. D.; and Lepage, A., "Reinforced Concrete Coupling Beams with High-Strength Steel Bars (SM Report No. 143)," The University of Kansas Center for Research, Lawrence, KS, 2020, 598 pp. https://hdl.handle.net/1808/30647.

16. Harries, K. A.; Mitchell, D.; Cook, W. D.; and Redwood, R. G., "Seismic Response of Steel Beams Coupling Concrete Walls," *Journal of Structural Engineering*, ASCE, V. 119, No. 12, 1993, pp. 3611-3629. doi: 10.1061/(ASCE)0733-9445(1993)119:12(3611)

17. Harries, K. A.; Gony, B.; and Shahrooz, B. M., "Behavior and Design of Reinforced Concrete, Steel, and Steel-Concrete Coupling Beams," *Earthquake Spectra*, V. 16, No. 4, 2000, pp. 775-799. doi: 10.1193/1.1586139

18. Bower, O. J., "Analytical Investigation into the Effect of Axial Restraint on the Stiffness and Ductility of Diagonally Reinforced Concrete Coupling Beams," MS thesis, University of Cincinnati, Cincinnati, OH, 2008, 108 pp.

19. Barbachyn, S. M.; Kurama, Y. C.; and Novak, L. C., "Analytical Evaluation of Diagonally Reinforced Concrete Coupling Beams under Lateral Loads," *ACI Structural Journal*, V. 109, No. 4, July-Aug. 2012, pp. 497-507.

20. Malcolm, R. C.; Bull, D. K.; Henry, R. S.; and Ingham, J. M., "The Effects of Axial Restraint in Reinforced Concrete Coupling Beams," *Proceedings*, New Zealand Concrete Industry Conference, Taupo, New Zealand, 2014, pp. 150-159.

21. Teshigawara, M.; Kato, M.; Sugaya, K.; and Matsushima, Y., "Energy Absorption Mechanism and the Fluctuation of Shear Force in the Coupled Shear Walls (Paper Number T-186-5)," *Proceedings*, Structural Engineers World Congress, San Francisco, CA, 1998.

22. ACI Committee 318, "Building Code Requirements for Structural Concrete (ACI 318-14) and Commentary (ACI 318R-14)," American Concrete Institute, Farmington Hills, MI, 2014, 520 pp.

23. Poudel, A.; Lequesne, R. D.; and Lepage, A., "Diagonally Reinforced Concrete Coupling Beams: Effects of Axial Restraint (SL Report 18-3)," The University of Kansas Center for Research, Lawrence, KS, 2018, 48 pp. https://hdl.handle.net/1808/26713.

24. Ameen, S.; Lequesne, R. D.; and Lepage, A., "Diagonally-Reinforced Concrete Coupling Beams with High-Strength Steel Bars (SM Report No. 138)," The University of Kansas Center for Research, Lawrence, KS, 2020, 346 pp. https://hdl.handle.net/1808/30314.

25. ASTM C39/C39M-17a, "Standard Test Method for Compressive Strength of Cylindrical Concrete Specimens," ASTM International, West Conshohocken, PA, 2017.

26. ASTM A706/A706M-15, "Standard Specification for Deformed and Plain Low-Alloy Steel Bars for Concrete Reinforcement," ASTM International, West Conshohocken, PA, 2015.

27. ASTM A1035/A1035M-16a, "Standard Specification for Deformed and Plain, Low-Carbon, Chromium, Steel Bars for Concrete Reinforcement," ASTM International, West Conshohocken, PA, 2016.

28. ASTM A370-17, "Standard Test Methods and Definitions for Mechanical Testing of Steel Products," ASTM International, West Conshohocken, PA, 2017.

29. ASTM E8/E8M-16ae1, "Standard Test Methods for Tension Testing of Metallic Materials," ASTM International, West Conshohocken, PA, 2016.

30. Lequesne, R. D., "Behavior and Design of High-Performance Fiber-Reinforced Concrete Coupling Beams and Coupled-Wall Systems," PhD dissertation, University of Michigan, Ann Arbor, MI, 2011, 277 pp.

NEW Symposium Publications from ACI

SP-347: Recent Developments in High Strain Rate Mechanics and Impact Behavior of Concrete

This Symposium Volume reports on the latest developments in the field of high strain rate mechanics and behavior of concrete subject to impact loads. This effort supports the mission of ACI Committee 370 “Blast and Impact Load Effects” to develop and disseminate information on the design of concrete structures subjected to impact, as well as blast and other short-duration dynamic loads.

Available in PDF format: $69.50
(ACI members: $39.00) ($30.50 savings)

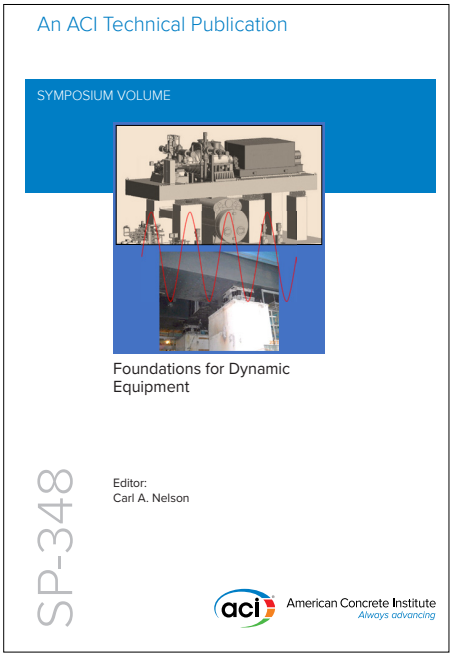

SP-348: Foundations for Dynamic Equipment

This special publication grew out of the Technical Session titled “Application of ACI 351-C Report on Dynamic Foundations,” held at the ACI Spring 2019 Convention in Québec City, Québec. Following this event, Committee 351 decided to undertake a special publication with contributions from those session participants willing to develop their presentations into full-length papers. Three papers included in the current publication were contributed by these presenters and their coauthors, with six additional papers provided by others.

Available in PDF format: $69.50
(ACI members: $39.00) ($30.50 savings)

American Concrete Institute
+1.248.848.3700 • www.concrete.org